Dalton Transactions

Accepted Manuscript

ROYAL SOCIETY OF CHEMISTRY

www.rsc.org/dalton

Dalton Transactions

RSCPublishing

ARTICLE

Highly bright multicolour emission through energy migration in core/shell nanotubes

Cite this: DOI: 10.1039/x0xx00000x

Lu Liu,[a] Nannan Zhang,[a] Zhihua Leng,[a] Yimai Liang,[a] Ruiqing Li,[a] Lianchun Zou,[*b] Shucai Gan[*a]

Received ooth January 2012,
Accepted ooth January 2012

DOI: 10.1039/x0xx00000x

www.rsc.org/

This paper describes a simple and environmentally-friendly approach that allowed for the facile synthesis of a gadolinium-based core/shell/shell nanotube structure with a set of lanthanide ions incorporated into separated layers. Additionally, by the rational design of a core/shell structure we systematically investigate the luminescence properties of different lanthanide ions in $NaGdF_4$ host, and efficient down-conversion emission can be realized through gadolinium sublattice-mediated energy migration. The Gd^{3+} ions play an intermediate role in this process. By changing the doped lanthanide ions, we generated multicolour emissions from the luminescent Ln^{3+} centers via energy transfer of $Ce^{3+}\rightarrow Gd^{3+}\rightarrow Ln^{3+}$ and $Ce^{3+}\rightarrow Ln^{3+}$ (Ln = Eu, Tb, Dy and Sm) in separated layers. Due to the strong absorption of ultraviolet (UV) irradiation by Ce^{3+} ions, the luminescence efficiency could be enhanced after doped Ce^{3+} ions in the shell. In $NaGdF_4$:5% Eu^{3+}@$NaGdF_4$@$NaGdF_4$:5% Ce^{3+} core/shell/shell nanotubes, with increasing the $NaGdF_4$ interlayer thickness, a gradual decrease in emission intensity was observed for the Eu^{3+} activator.

1. Introduction

One-dimensional (1D) nanostructures have attracted considerable interest since the discovery of carbon nanotubes (CNTs).[1] They could act as electrically, magnetically, or optically functional host materials due to their unusual properties amplified by their marked shape-specific and quantum-confinement effects. The development of nanomaterials for luminescence imaging is an area that is currently attracting extensive interests across a wide range of science, biomedical disciplines,[2] engineering. Lanthanide ion-doped luminescent materials have been widely investigated due to the fascinating optical characteristics based on their unique intraconfigurational f-f transitions, which are weakly dependent on the crystal field or coordination environment. To date, the main routes developing for synthesizing lanthanide (Ln^{3+}) ions doped nanocrystals (NCs) in solution include co-precipitation, solution-phase method, thermal decomposition, and hydrothermal method.[3-6] As a typical solution-based approach, hydrothermal method has been proven to be an environmentally friendly acceptable process with relatively high yield of desired products. The advantages in synthesis techniques make it possible to synthesize not only the spherical shape NCs but also a variety of other shapes, such as disk, wire, hexagon, raisin, rod, tube, etc.[7-13] Photoluminescence (PL) nano-materials with different morphologies being used for bioassay have became common, useful tools. Several classes of luminescent materials, including organic fluorescent dyes,[14] quantum dots (QDs),[15-17] harmonic nanoparticles,[18] graphene oxide,[19] and lanthanide-doped NCs,[20-23] have been developed and exploited for biological labelling. In contrast to conventional luminescent materials, lanthanide-doped nanophosphors exhibit excellent optical and chemical properties including sharper emission bandwidth, photostability, no photoblinking, and low toxicity.

NCs have small particle size and high surface-to-volume ratio that supply the emission control with more tunable parameters. However, the remarkably lower luminescent efficiency compared to bulk materials has hindered the development and application of NCs. To overcome this drawback, a core/shell structure has been developed to minimize the surface-quenching-induced emission losses and proven to enhance the PL intensity especially for the active shell. In the early 1990s, researchers synthesized concentric multilayer semiconductor nanoparticles with the view to improving the property of the semiconductor materials.[24] Core/shell NCs are gradually attracting more and more attention, there are large varieties of core/shell NCs available so far with a wide range of applications.[25-29] When coating of the shell material, the properties of the core particle such as thermal stability, reactivity or optical property can be modified. Energy transfer among sensitizer, intermediate and emitter ions can also be investigated in detail by introducing the core/shell nanostructure.[30, 31] Hence many efforts have been devoted to investigate such PL process in many host lattices,[32-36] especially in the gadolinium compounds. Hexagonal-phase $NaGdF_4$ was chosen as the host owing to its ability to render high efficiency and the low phonon energy and high photochemical stability. Furthermore, the Gd^{3+} host ion that features half-filled 4f orbitals is relatively inert in the luminescence process and can act as an intermediate to allow energy to migrate over the Gd^{3+} sublattice, and in this case it is possible to excite all these materials by a single wavelength irradiation. Importantly, the

lowest excited $^6P_{7/2}$ level of Gd^{3+} ion is situated in the UV spectral region, where most of the lanthanide ions have overlapping absorption bands. As is known that lanthanide-doped luminescent materials can show multicolor emissions just by changing the dopants.

In this investigation, PL studies of $NaGdF_4$:Ln^{3+}@$NaGdF_4$@$NaGdF_4$:Ce^{3+} core/shell/shell nanotubes (NTs) doped with a series of lanthanide ions have been undertaken to confirm the occurrence of efficient energy transfer from Ce^{3+} to Gd^{3+} and then to Ln^{3+}. The design of core/shell/shell nanostructure for management of energy transition is depicted in Figure 1, photoexcitation takes place in the harvesting layer, then energy exchange interactions are mediated by arrays of Gd^{3+} migrator ions that can transport the energy from outermost shell to the tunning layer while filtering unwanted cross relaxations. To confirm the dominant effect of $NaGdF_4$ host lattice in mediating energy migration and evaluate the contribution of Ce^{3+} to the emission process of these lanthanide activators and in a further attempt to probe energy migration from Ce^{3+} to Gd^{3+}, we have investigated a series of core/shell (and core/shell/shell) NCs.

2. Experimental

2.1. Chemicals and Materials

The rare earth oxides Ln_2O_3 (99.99%) (Ln = Y, Gd, Eu, Dy, Sm) and Tb_4O_7 (99.99%) as well as $Ce(NO_3)_3{\cdot}6H_2O$ (99.95%) were purchased from Shanghai Reagent Co. (China). Sodium hydroxide (NaOH), hydrogen fluoride (HF), sodium fluoride (NaF) and hydrogen Chloride (HCl) were purchased from Beijing Chemical Co., other chemicals were purchased from Beijing Beihua Fine Chemicals Co. All chemicals are of analytical grade reagents and used directly without further purification. Rare earth nitrates except $Ce(NO_3)_3$ were prepared by dissolving the corresponding metal oxide in nitric acid solution under heating with agitation. All of the doping ratios of Ln^{3+} are in mole equivalents in our experiments. Deionized water was used throughout.

2.2. Synthesis of $Gd(OH)_3$ NTs

Rare earth hydroxide NTs were hydrothermally prepared from corresponding nitrates in the presence of alkali. In a typical synthesis, 1 mmol $Gd(NO_3)_3$ aqueous solution was first added into 25 mL of deionized water under vigorous stirring to form a clear solution in a beaker, followed by the dropwise add of NaOH solution until it reached pH 11.5, and the white precipitate was obtained. After additional agitation for 15 min, the colloidal precipitate (total volume = 35 ml) was transferred into a stainless Teflon-lined autoclave (50 mL) and heated at 130 ^oC for 6 h. The resulting white precipitate was collected, centrifuged, and washed with deionized water and ethanol for several times respectively and finally dried at 80 ^oC for 6 h in a vacuum oven. $Gd(OH)_3$:5% Ln^{3+} (Ln = Eu, Tb, Dy and Sm) NTs were prepared by the same procedure, except for adding additional 5% $Ln(NO_3)_3$ into the solution of $Gd(NO_3)_3$ at the initial stage.

2.3. Synthesis of $NaGdF_4$ NTs

For a typical synthesis, 0.2083 g of $Gd(OH)_3$ NTs prepared as above was redispersed into 25 ml deionized water by ultrasonic and vigorous stirring for 1 h, at the same time, 0.1890 g of NaF and 0.3000 g of HF (40%) were dissolved in 10 mL of deionized water with stirring for 30 min, then mixed the above two solutions, followed by further stirring for 30 min. After that, the final solutions (total volume = 35 ml) were placed into a 50 ml Teflon-lined stainless steel autoclave and heated at 130 ^oC for 12 h. The powders of the $NaGdF_4$ NCs were finally obtained after being washed with deionized water and alcohol several times and dried at 80 ^oC for 6 h in a vacuum oven.

2.4. Synthesis of $NaGdF_4$@$NaGdF_4$ core/shell NTs

For the growth of $NaGdF_4$ shell on the ultrasmall $NaGdF_4$ cores, 0.2562 g of $NaGdF_4$ NTs prepared as above was redispersed into 20 ml deionized water by ultrasonic and vigorous stirring for 1 h, 0.5 mmol $Gd(NO_3)_3$ was added into the above solution with stirring for 30 min, then 15 ml solution containing NaF (2.25 mmol) was added and the resulting mixture was stirred for another 30 min. Finally, the mixture solution was transferred into a stainless steel autoclave and heated at 130 ^oC for 12 h and then cooled down to room temperature. The precipitate was washed with deionized water and alcohol several times and dried at 80 ^oC for 6 h in a vacuum oven.

2.5. Synthesis of $NaGdF_4$@$NaGdF_4$@$NaGdF_4$ core/shell/shell NTs

$NaGdF_4$@$NaGdF_4$@$NaGdF_4$ NTs were hydrothermally prepared with the same method as the core/shell nanostructures described above except for adding additional $NaGdF_4$@$NaGdF_4$ into the solution as the template at the epitaxial growth stage.

2.6. Characterization

Powder X-ray diffraction (XRD) patterns were measured on a Rigaku D/max-II B X-ray diffractometer at a scanning rate of 5^o/min in the 2θ range from 10^o to 80^o with monochromatic Cu-Kα radiation (wavelength λ = 1.5418 Å). Images of the as-synthesized products were characterised by a field emission scanning electron microscope (FE-SEM, Hitachi, S-4800) with an energy-dispersive X-ray spectrometer (EDS). The size and structure of the synthesized NTs were observed by using a Hitachi 8100 transmission electron microscope (TEM, Hitachi, Tokyo, Japan) and high-resolution transmission electron microscope (HRTEM), performed on a FEI Tecnai G2 S-Twin transmission electron microscope. Images were acquired digitally on a Gatan multiple CCD camera. The PL excitation and emission spectra were acquired by using a Hitachi F-7000 spectrophotometer fitted with a 150-W xenon lamp as the excitation source. All the measurements were performed at room temperature.

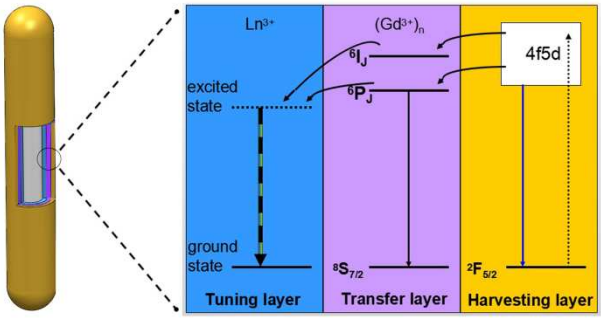

Figure 1. Schematic illustration of the energy transfer mechanism in the lanthanide-doped core/shell/shell nanostucture for management of complex energy transitions. Note that core and shell layers are highlighted with different background colors.

3. Results and discussion

3.1. Phase Identification

An XRD pattern of the obtained $Gd(OH)_3$ product is showed in Figure 2Aa. XRD pattern of as-synthesized $Gd(OH)_3$ NTs revealed that the products are pure hexagonal $Gd(OH)_3$ phase (space group of P63/m) with lattice constants a = 6.329 Å and c = 3.631 Å (JCPDS#97-020-0093). Figure 2B exhibited the crystal structure of hexagonal-phase $Gd(OH)_3$. The XRD pattern showed that the crystalline phase of the resulting products after fluorination is pure $NaGdF_4$ (JCPDS#00-027-0699) with lattice constants a = 6.020 Å and c = 3.601 Å, indicating that the hydroxide was converted to the corresponding fluoride by hydrothermal treatment (Figure 2Ab). The crystal structure of $NaGdF_4$ consists of an ordered array of F^- ions with two types of relatively low-symmetry cation sites selectively occupied by Na^+ and Gd^{3+} ions (Figure 2C), resulting in significant electron cloud distortion of the cations to accommodate the structural change. It was found that the crystal structure of the obtained $NaGdF_4$@$NaGdF_4$, $NaGdF_4$@$NaGdF_4$@$NaGdF_4$ NTs are all consistent with the structure of the core NTs, and well indexed to $NaGdF_4$ standard card (Figure 2Ac, d).

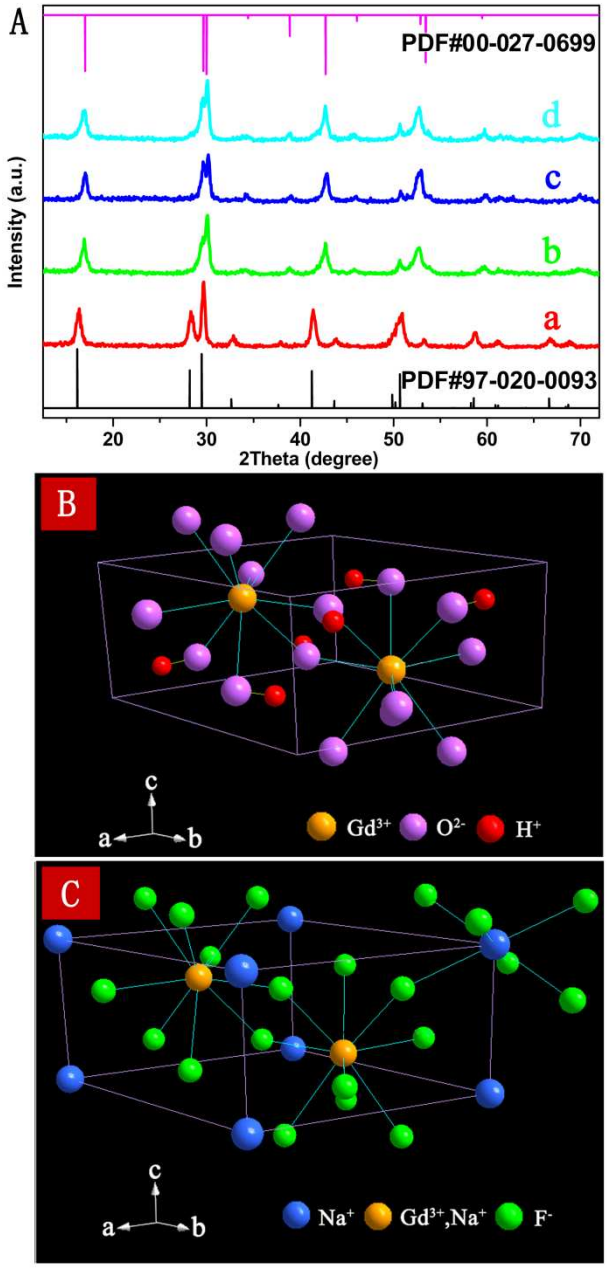

Figure 2. Powder XRD patterns of the as-synthesized $Gd(OH)_3$ nanotubes (a), and the $NaGdF_4$ composite samples prepared through hydrothermal in situ ion-exchange transformation approach (b), and the $NaGdF_4$@$NaGdF_4$ (c), $NaGdF_4$@$NaGdF_4$@$NaGdF_4$ (d) nanotubes; Schematic presentation of hexagonal-phase $Gd(OH)_3$ (B) and hexagonal-phase $NaGdF_4$ structures (C), respectively.

The ionic radii for the nine-coordinated Gd^{3+}, Eu^{3+}, Tb^{3+}, Dy^{3+} and Sm^{3+} are 1.107, 1.120, 1.095, 1.083 and 1.132 Å, respectively.[37] Thus, due to the same valence and similar ionic radius, the RE ion dopants (Ln^{3+}) are expected to replace Gd^{3+} sites. Figure S1 presented the XRD patterns of Ln^{3+} ions doped $NaGdF_4$, where the diffraction peaks also matched well with those of $NaGdF_4$ standard card. No additional impurity peaks corresponding to other phases have been found, indicating that Ln^{3+} ions have been effectively doped into the $NaGdF_4$ host lattice and the doping did not cause any significant change in the host structure.

3.2. Formation Mechanism of the $NaGdF_4$@$NaGdF_4$@$NaGdF_4$ NTs

To understand the detailed evolution process of the nanotube structure, time-resolved SEM images of $Gd(OH)_3$ NTs synthesized under different reaction times were taken. The corresponding XRD patterns and the SEM images of the intermediates obtained under different reaction time intervals were shown in Figure S2 and Figure S3, respectively. At the early stage of the synthesis process, OH^- ions interact with Gd^{3+} ions to form hexagonal $Gd(OH)_3$ nanocrystal nuclei. Increasing evolution time to 10 min, the growth direction of the NTs occurs preferentially along the [001] direction (c-axis) still with poor uniformity. With increasing the reaction time to 1 h, a significant change in the morphology of the products happened, favors the formation of products constructed by few particles and NTs. As shown in Figure S2f, pure hexagonal-phase $Gd(OH)_3$ could be successfully obtained when the reaction time was increased from 1 h to 6 h. As shown in Figure 3, we present the well organized assembly of zero dimensional (0D) nanoparticles into 1D NTs arrays. On the basis of the above analyses, it can be concluded that the nanocrystal evolves from nanoparticles to mixed morphology and ultimately to NTs with the increase of reaction time. Moreover, the intensities of these diffraction peaks increase significantly with the increase of reaction time, illustrating that the crystallinity of the samples

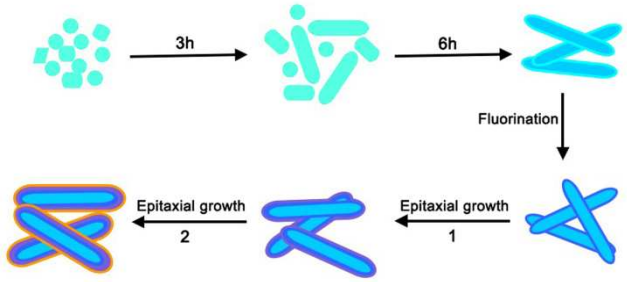

Figure 3. Schematic illustration for the formation process of $NaGdF_4$@$NaGdF_4$@$NaGdF_4$ nanotubes. 1) the first shell deposition. 2) the second shell deposition.

increases with the further reaction (Figure S2).
Then the in-situ ion-exchange route to synthesize $NaGdF_4$ NTs under different conditions was used to investigate process

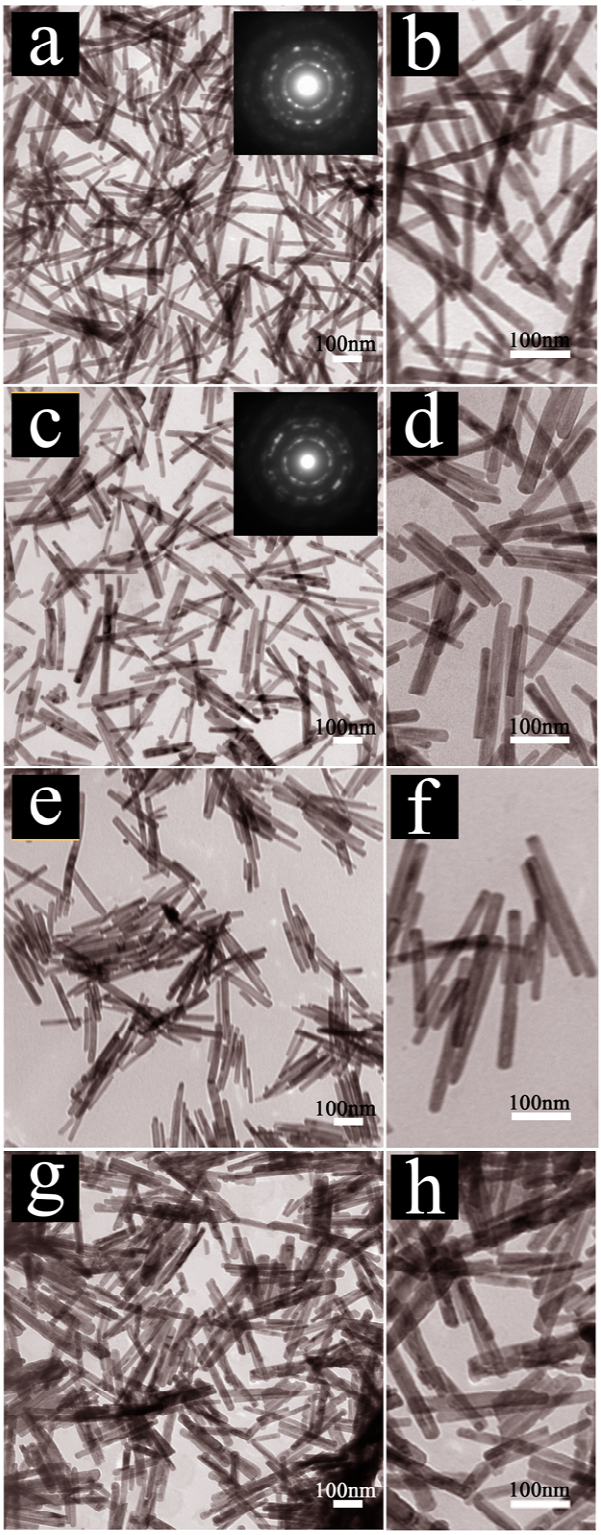

Figure 4. Typical transmission electron microscopy (TEM) images of the as-synthesized nanotubes: $Gd(OH)_3$ and corresponding SAED patterns (inset) (a, b); $NaGdF_4$ and corresponding SAED patterns (inset) (c, d); $NaGdF_4$@$NaGdF_4$ core/shell nanostructures (e, f); $NaGdF_4$@$NaGdF_4$@$NaGdF_4$ core/shell/shell nanostructures (g, h).

of transforming $Gd(OH)_3$ into $NaGdF_4$ NTs.[38] The $NaGdF_4$ NTs can be obtained after in-situ acid corrosion and ion exchange process by reaction of $Gd(OH)_3$ precursors with HF and NaF under hydrothermal conditions at 130 ^oC for 12 h. In this process $Gd(OH)_3$ precursors were employed as both the physical and chemical templates, which not only keep the morphology of the precursors but also afford Gd^{3+} source. Temperature plays a critical role in controlling the crystal phase of the final products. When the reaction temperature is too high, the products morphology would change, tube-like $NaGdF_4$ products cannot be yielded when the temperature is too low even with a long reaction time.[38]

When the reaction was carried out in the absence of HF, under other equal reaction conditions, XRD result showed that the $Gd(OH)_3$ phase had no change at all (Figure S4a). XRD patterns shown in Figure S4b-d, the hexagonal phase of $Gd(OH)_3$ gradually reduces and the hexagonal phase of $NaGdF_4$ gradually grows with increasing the HF to $Gd(OH)_3$ ratio. As the ratio increased to 6:1, the $Gd(OH)_3$ NTs could completely transformed into $NaGdF_4$, clearly illustrating that the hydrothermal in-situ ion exchange process occurs. No other impurity peaks corresponding to $Gd(OH)_3$ were observed, indicating that all $Gd(OH)_3$ transformed completely into $NaGdF_4$. During this hydrothermal in-situ ion-exchange process, HF first corrodes $Gd(OH)_3$ NTs. Then F^- ions can substitute OH^- ions and interact with Gd^{3+} ions to form a more stable phase. However, in the $NaGdF_4$ crystals, Na^+ ions are randomly dispersed in different sites, so they can be easily trapped into the crystals to form a more stable $NaGdF_4$ phase. During the process of fluoride, the positions and arrangements of Gd atoms remain unchanged since the hexagonal $Gd(OH)_3$ and $NaGdF_4$ have a similar crystal structure. Thus, this in-situ ion-exchange approach insures the complete retention of morphology of the $Gd(OH)_3$ precursors. In comparison to that of $Gd(OH)_3$ NTs precursors, the diameter of $NaGdF_4$ NTs increases slightly, which is ascribed to the lattice constant changes. The thermodynamic driving force should be a key to the formation of $NaGdF_4$ via the hydrothermal in-situ ion-exchange approach, because the structure of the $NaGdF_4$ is more stable than that of $Gd(OH)_3$. Figure 4a-d showed the TEM images of as-prepared $Gd(OH)_3$ and $NaGdF_4$ NTs, revealed that the corresponding shape was fairly uniform NTs. In addition to the core-only NTs, core/shell NTs with tunable shell thickness were obtained through epitaxial growth of $NaGdF_4$ shells on the core NTs. Figure 4e-h showed the TEM of the final phase of the synthesis of $NaGdF_4$@$NaGdF_4$ and $NaGdF_4$@$NaGdF_4$@$NaGdF_4$ samples. The dimension parameters of these samples were shown in Table 1 (Supplementary Information).

To better understand the in-situ ion-exchange process, experiment was also carried out in the presence of HCl and NaF. In the absence of HCl, but only NaF, the pure $NaGdF_4$ was not obtained. XRD result showed that the $Gd(OH)_3$ phase had almost no change until the ratio increased to 3:1 (Figure S6). With increasing the ratio to 3:1, a significant change in the XRD pattern of the products happened, indicating that $Gd(OH)_3$ transformed partly into $NaGdF_4$. It was because the free F^- combines with H^+ to create HF a weak acid that makes it possible to enter into the lattice to react with $Gd(OH)_3$. Further increasing the $HCl/Gd(OH)_3$ ratio to 6:1, the pure GdF_3 was finally obtained as shown in Figure S6. HCl is a strong acid produced much H^+ in solution, so the $Gd(OH)_3$ NCs reacts with extra free H^+ ions to form Gd^{3+}. After that, Gd^{3+} will combines with F^- to form the pure GdF_3 (PDF#00-012-0788), which causes the change of the morphology from NTs to

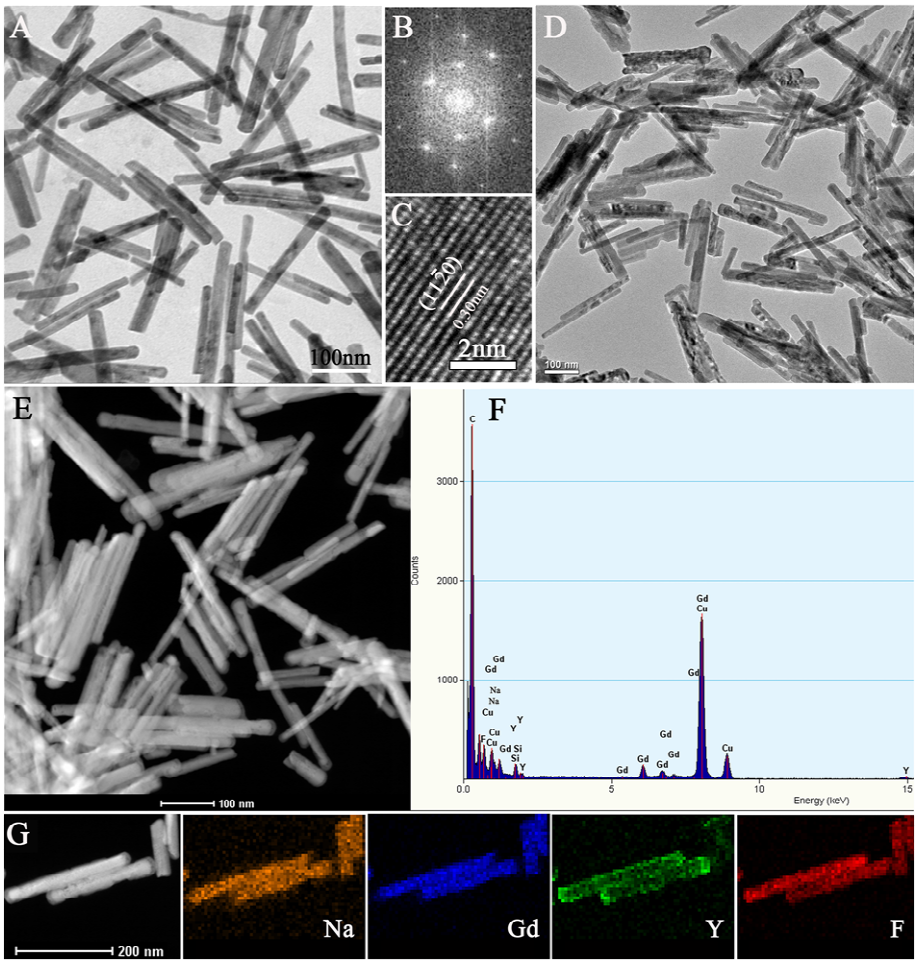

Figure 5. (A-C) TEM image and corresponding fast Fourier transform (FFT), HRTEM images of the as-synthesized $NaGdF_4$. (D) TEM image of the as-synthesized $NaGdF_4$@$NaYF_4$. (E, F) HADDF-STEM image and EDS spectrum of $NaGdF_4$@$NaYF_4$ core/shell nanostructure, and (G) EDS mapping of Na, Gd, Y and F of $NaGdF_4$@$NaYF_4$ NCs.

micro-flowers as is shown in Figure S5.

We employed a $NaGdF_4$@$NaYF_4$ core/shell nanostructure to separated the Gd^{3+}, Ln^{3+} ions in core and shell respectively. Energy-dispersive X-ray spectrometer (EDS) showed a characteristic intensity profile of Na, Gd, Y and F elements, suggesting $NaGdF_4$@$NaYF_4$ NCs were obtained (Figure 5F). The high angle annular dark field scanning transmission electron microscopy (HAADF-STEM) image was employed to identify the core/shell structures. The HAADF-STEM image showed a discernible contrast, indicating the formation of the core/shell structures (Figure 5E). The elemental mapping images in which distributing Na, Gd, Y and F elements further confirming its core/shell structure (Figure 5G). After doped with Ln^{3+}, energy-dispersive X-ray spectrometer (EDS) of $NaGdF_4$@$NaYF_4$:5% Ln^{3+} also showed a characteristic intensity profile of Eu^{3+}, Tb^{3+}, Dy^{3+} and Sm^{3+} element, further suggesting $NaGdF_4$@$NaYF_4$:5% Ln^{3+} NCs were obtained (Figure S7).

3.3. Photoluminescent Properties of Ln^{3+} Doped NCs

To confirm the dominant effect of $NaGdF_4$ host lattice in mediating energy migration and subsequent transfer to the activators, we compared the optical property of the $NaGdF_4$@$NaYF_4$:5% Ln^{3+} NTs with that of Ln^{3+} doped $NaGdF_4$ NTs. As shown in Figure 6 that under a single-wavelength excitation of 271 nm ($^8S_{7/2}\rightarrow{}^6I_J$ transition of Gd^{3+}) in the UV region, a sharp line emission at about 310 nm can be observed for all $NaGdF_4$@$NaYF_4$:5% Ln^{3+} samples, which is ascribed to the Gd^{3+} $^6P_J\rightarrow{}^8S_{7/2}$ transition. The emission peaks between 400-750 nm are clearly assigned to the characteristic optical transitions of Eu^{3+} ($^5D_0\rightarrow{}^7F_J$, J = 0-5; $^5D_1\rightarrow{}^7F_J$, J = 0-2), Tb^{3+} ($^5D_3\rightarrow{}^7F_J$, J = 6-4; $^5D_4\rightarrow{}^7F_J$, J = 6-3), Dy^{3+} ($^4F_{9/2}\rightarrow{}^6H_{15/2}$, $^6H_{13/2}$) and Sm^{3+} ($^4G_{5/2}\rightarrow{}^6H_{J/2}$, J = 5, 7, 9), respectively. The assignments of these emissions are summarized in table 2 (Supplementary Information). In other words, the emission spectra exhibit the representative emission of Gd^{3+} and Ln^{3+}, indicating that the energy transfer from Gd^{3+} to the Ln^{3+} luminescent centers has occurred. The $NaGdF_4$ samples doped with different lanthanide ions show multicolor visible emissions.

The Ln^{3+} characteristic emission intensity of the $NaGdF_4$:5% Ln^{3+} NCs are much stronger than that of the $NaGdF_4$@$NaYF_4$:5% Ln^{3+} samples, this can be attributed to the

Dalton Transactions RSCPublishing

ARTICLE

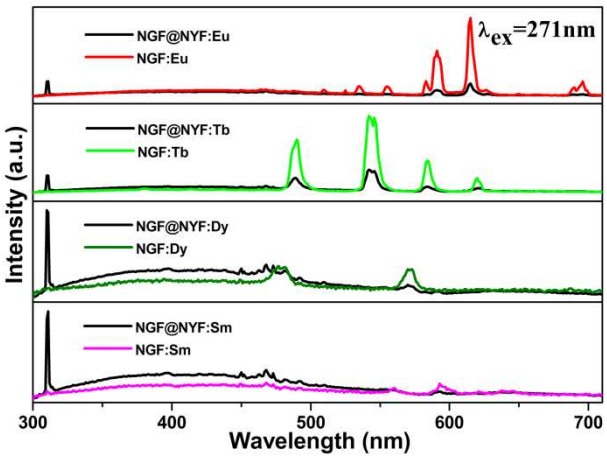

Figure 6. Comparative spectroscopic studies of the $NaGdF_4$:5% Ln^{3+} nanotubes with $NaGdF_4$@$NaYF_4$:5% Ln^{3+} nanotubes. Note that $NaGdF_4$ and $NaYF_4$ were abbreviated as NGF, NYF, respectively.

suppression of the energy migration process from Gd^{3+} to Ln^{3+} activator ions by Y^{3+} in the shell structure. The PL intensity at 310 nm of the Gd^{3+} ions in $NaGdF_4$:5% Ln^{3+} were much weaker than that of $NaGdF_4$@$NaYF_4$:5% Ln^{3+}, which indicated that the trapping of excitation energy by the activator ions was not very efficient. This can be ascribed to the spectral overlap between the emission spectrum of the sensitizer and the absorption (excitation) spectrum of the activator. Because both Eu^{3+} and Tb^{3+} show absorption bands in the spectral region where Gd^{3+} emits, the Gd^{3+} emissions intensity in these two cases are insignificant. For Sm^{3+} and Dy^{3+} activators, we noticed that the ability of these two activators in the shell to trap the energy of Gd^{3+} is quite weak, arising from the presence of many closely spaced energy levels. Take Sm^{3+} as an example, Sm^{3+} ions may transfer part of its energy in its $^4G_{5/2}$ excited-state to the ground-state of neighboring Sm^{3+} ions through cross-relaxation, resulting in these both ions occupying the $^6F_{9/2}$ energy level and then nonradiative relaxation to the ground state. Especially when Sm^{3+} at a high concentration level, this effect is particularly pronounced. Meanwhile Dy^{3+} and Sm^{3+} do not show well matched transitions where Gd^{3+} levels are situated, indicating that the energy transfer from Gd^{3+} to the Dy^{3+} and Sm^{3+} luminescent centers is incomplete, so the ratio of Gd^{3+} emissions to the total luminescence are consequently higher, by contrast.

We presented the standard emission spectra of $NaGdF_4$ and $NaGdF_4$@$NaGdF_4$:5% Ce^{3+} acquired under the excitation of 251 nm (4f-5d transition of Ce^{3+}) and exitation spectra of the as-prepared $NaGdF_4$:5% Ln^{3+} (Ln = Eu, Tb, Dy and Sm) (Figure S8). This figure showed that there is a overlap between the emission spectrum of the sensitizer and the absorption (excitation) spectrum of the activator. A broad and intense emission between 340 and 550 nm is observed in pure $NaGdF_4$ NTs, which may assign to PL originating from defect impurities or surface states in the $NaGdF_4$ matrix.[39] The shoulder peaks between 430 and 500 nm of $NaGdF_4$ are considered to be produced by the Xenon lamp. In general, defects exist in crystals that provide nonradiative relaxation paths are unintentional and therefore are always distributed uniformly throughout the phosphors. The mechanisms for the defects emission are complicated and not totally understood. The emission structures of the $NaGdF_4$@$NaGdF_4$:5% Ce^{3+} NTs invoke possible presence of Gaussian components. The decomposition of the broad band into individual Gaussian components has two Gaussians. The energy transfer between activator pairs or between sensitizers and activators is highly sensitized to the defects in the crystal lattices. For nanosized crystal, the surface crystal lattices were broken down by high density of defects that interrupts the energy transfer routes between activator pairs/or between sensitizers and activators. It has been observed that with doping the Ce^{3+} ions into the $NaGdF_4$ matrix, a broad band of Ce^{3+} emission (5d-4f transition) between 300 and 430 nm, as well as a sharp line of Gd^{3+} emission ($^6P_{7/2}$→$^8S_{7/2}$ transition) at 310 nm and defect related emission can be observed, indicating that the energy transfer from Ce^{3+} to Gd^{3+} ions is occurred.

Figure 7 showed the exitation and emission spectra of $NaGdF_4$:5% Ln^{3+}@$NaGdF_4$:5% Ce^{3+} (Ln = Eu, Tb, Dy and Sm) NTs, respectively. Though direct energy transfer from Ce^{3+} ions to activator ions can also occur, sometimes, direct sensitization of some lanthanide ions by Ce^{3+} is not available. For example, Ce^{3+} and Eu^{3+} are known to quench each other's emission due to electron transfer quenching (Ce^{3+}+Eu^{3+} → Ce^{4+}+Eu^{2+}), therefore energy transfer from Ce^{3+} to Eu^{3+} has to occur via the Gd^{3+} sublattice. To regulate energy exchange interaction between the sensitizer and the activator, the sensitizer and the activator are spatially confined in different layers of the core/shell structure, which is necessary for eliminating deleterious quenching. Electronic transitions within $4f^n$ configurations of Tb^{3+} ions are strongly forbidden that they appear with very weak intensity in the absorption spectra.[37] However, the emission efficiency of Tb^{3+} activator can be

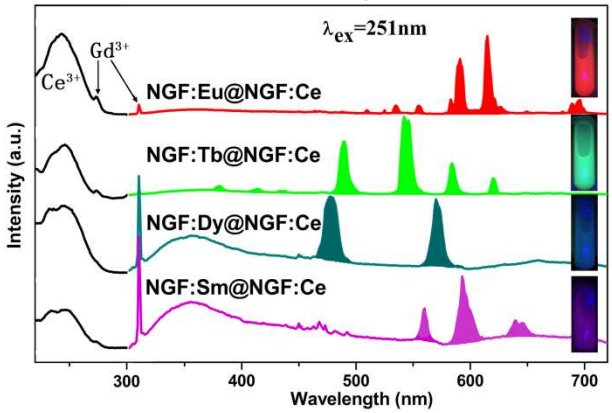

Figure 7. Exitation and emission spectra of the as-prepared $NaGdF_4$:Ln^{3+}@$NaGdF_4$:Ce^{3+} and their corresponding photographs under 254 nm UV lamp (inset). Note that these nanotubes were dispersed in ethanol solution and the concentration is about 4 mg·ml^{-1}.

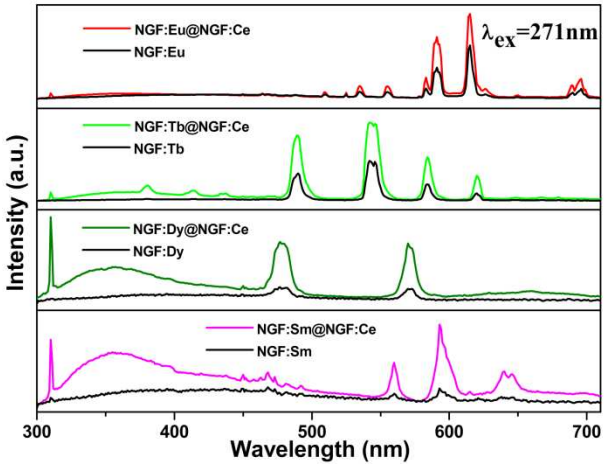

Figure 8. Emission spectra of the as-prepared $NaGdF_4$:5% Ln and $NaGdF_4$:5% Ln^{3+}@$NaGdF_4$:5% Ce^{3+} nanoparticles (Ln = Eu, Tb, Dy and Sm).

greatly improved by exciting a different ion (sensitizer, i.e., Ce^{3+}) with an allowed electronic transition which transfers the excitation energy to the rare earth activators (i.e., Tb^{3+}). Therefore, the energy transfer processes from sensitizer to activator can enhance the Tb^{3+} green emission in $NaGdF_4$:5% Tb^{3+}@$NaGdF_4$:5% Ce^{3+} NTs. For the Dy^{3+} and Sm^{3+} doped core@shell samples, Ce^{3+} emission between 300 and 430 nm clearly be observed, which indicated that energy transfer in these samples were not so efficient as those of Eu^{3+} and Tb^{3+} doped samples.

During the fluorescence process, the excitation energy is first absorbed by the 4f-5d transition of Ce^{3+} in the shell and transferred to the Gd^{3+} and migrates over the Gd^{3+} sublattice, finally, trapping of the migrating energy occurs at Ln^{3+} (Ln = Eu, Tb, Dy and Sm) in the core, where the energy is released as fluorescent emissions. Therefore, a sharp line of Gd^{3+} emission at about 310 nm and the emission peaks of the $NaGdF_4$:5% Ln^{3+}@$NaGdF_4$:5% Ce^{3+} generate from the 4f-4f transition of Ln^{3+} ions can be observed.

To evaluate the contribution of Ce^{3+} to the emission process of these lanthanide activators and in a further attempt to probe energy transfer from Ce^{3+} to Gd^{3+} in the energy migration process, We compared the optical property of the $NaGdF_4$:5% Ln^{3+} with $NaGdF_4$:5% Ln^{3+}@$NaGdF_4$:5% Ce^{3+} core/shell nanotructure under the excitation of 271 nm (Figure 8). Due to the strong absorption in the wavelength range between 200 and 300 nm resulting from the allowed 4f-5d transition of Ce^{3+}, Ce^{3+} ions were incorporated in the shell layer and used to harvest the UV excitations. Apparently, we can observed significant emission enhancement for $NaGdF_4$:5% Ln^{3+}@$NaGdF_4$:5% Ce^{3+} NCs. Energy transfer in Dy^{3+} and Sm^{3+} doped samples are not so efficient as those of Eu^{3+} and Tb^{3+} doped samples, therefore, the characteristic PL intensity of the Ln^{3+} (Ln = Dy and Sm) ions in $NaGdF_4$:5% Ln^{3+} was much weaker than the other two NCs. After the $NaGdF_4$:5% Ce^{3+} shell coating, we observed significant emission enhancement for $NaGdF_4$ products doped with Dy^{3+} and Sm^{3+}, respectively. The enhancement of the PL was further confirmed by fluorescence lifetime of the activators, which provided another important parameter other than PL intensity for the assay. Unlike the $NaGdF_4$:5% Ln^{3+} NCs, the $NaGdF_4$:5% Ln^{3+}@$NaGdF_4$:5% Ce^{3+} core/shell nanostructure presents a very slightly longer effective decay times (Figure 10). This

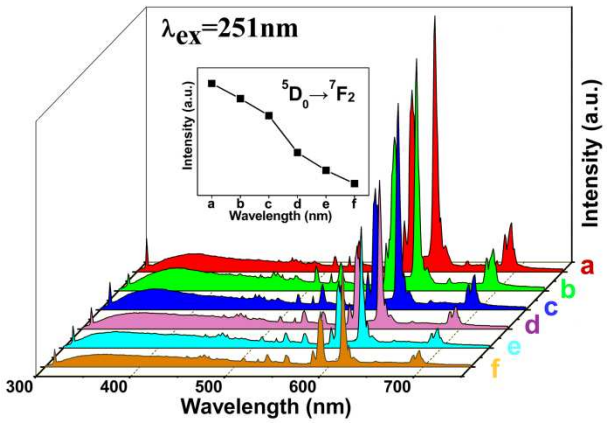

Figure 9. Emission spectra of $NaGdF_4$:5% Eu^{3+}@$NaGdF_4$@$NaGdF_4$:5% Ce^{3+} samples with $NaGdF_4$ different thickness. Epitaxial growth of the interlayer obtained under different core/shell ratios (moL/moL): 10:0 (a); 10:1 (b); 10:3 (c); 10:5 (d); 10:7 (e); 10:9 (f).

corresponds to an increase in the total emission intensity from the core-shell $NaGdF_4$:5% Ln^{3+}@$NaGdF_4$:5% Ce^{3+} NCs than from the $NaGdF_4$:5% Ln^{3+} NCs. This experimental fact indicated that the core/shell nanostructure modification in the $NaGdF_4$:5% Ln^{3+}@$NaGdF_4$:5% Ce^{3+} NCs can significant enhance luminescence intensity of different activator Ln^{3+} ions.

The migration of excitation energy through the Gd^{3+} sublattice may travel a substantial length. To shed more light on this effect, we next verified the critical role of the Gd^{3+} sublattice in the interlayer energy-transfer process by varying the interlayer thickness in the host lattice. Distance-dependent energy migration studies were carry on core/shell/shell nanostructure comprising a $NaGdF_4$:5% Eu^{3+} core, an undoped $NaGdF_4$ spacing layer, and a $NaGdF_4$:5% Ce^{3+} outer shell. To make a different spacing layer of $NaGdF_4$, we increasing the amount of the spacing layer precursor. Emission spectra of $NaGdF_4$:5% Eu^{3+}@$NaGdF_4$@$NaGdF_4$:5% Ce^{3+} nanostructure separated by a $NaGdF_4$ spacing layer of different thickness were obtained (Figure 9). Without the $NaGdF_4$ interlayer, we could observe intense Eu^{3+} emission, arising from close distance between sensitizer and activator ions. Close distance means energy migration from sensitizer and activator ions could be easier to realize. After coating of a $NaGdF_4$ spacing layer (core/shell ratios = 10:1), the emission intensity of Eu^{3+} was reduced a bit (Figure 9b). PL studies showed with further increase in the $NaGdF_4$ interlayer thickness, a gradual decrease in emission intensity was observed for the Eu^{3+} activator (Figure 9c-f). The decrease in the emission intensity of the Eu^{3+} ions in the core/shell/shell nanostructure largely results from the suppression of the energy transfer process by virtue of the increased Gd-Gd interionic distance. The important point is that energy transfer through Gd^{3+} sublattice can travel a substantial length without losing most of the excitation energy.

In order to better understand the energy transfer mechanisms, Figure 11 showed the energy level in the energy transfer process. As previously mentioned, the external UV light was absorbed by sensitizer (Ce^{3+}) and then transferred to intermediate ions (Gd^{3+}), followed by a transfer of this excited energy from Gd^{3+} to Ln^{3+} activator (Ln = Eu, Tb, Dy and Sm), in this process, Gd^{3+} sublattice provided a route or a bridge between sensitizer and activator ions. In addition, some of the excited energy can be transferred from Ce^{3+} to Ln^{3+} directly.

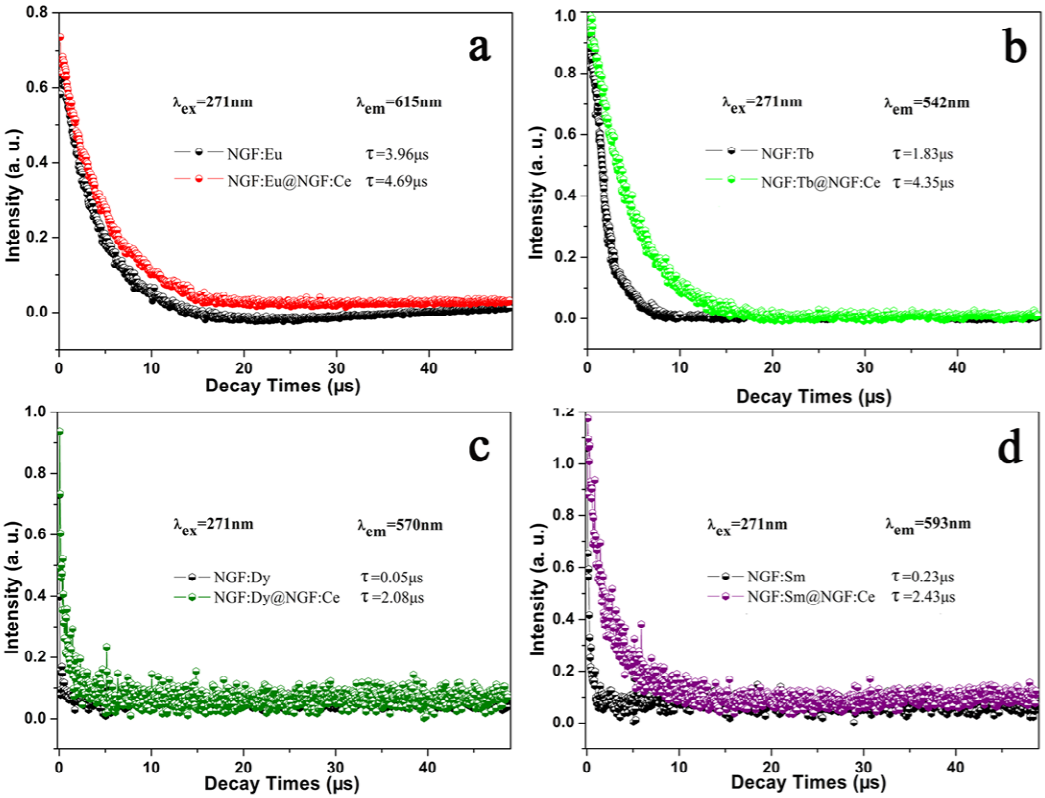

Figure 10. PL decay properties of $NaGdF_4$:5% Ln^{3+} NCs and $NaGdF_4$:5% Ln^{3+}@$NaGdF_4$:5% Ce^{3+} NCs. (a) PL decay curves of $^5D_0 \rightarrow {}^7F_2$ of Eu^{3+}, (b) PL decay curves of $^5D_4 \rightarrow {}^7F_5$ of Tb^{3+}, (c) PL decay curves of $^4F_{9/2} \rightarrow {}^6H_{13/2}$ of Dy^{3+}, (d) PL decay curves of $^4G_{5/2} \rightarrow {}^6H_{7/2}$ of Sm^{3+}.

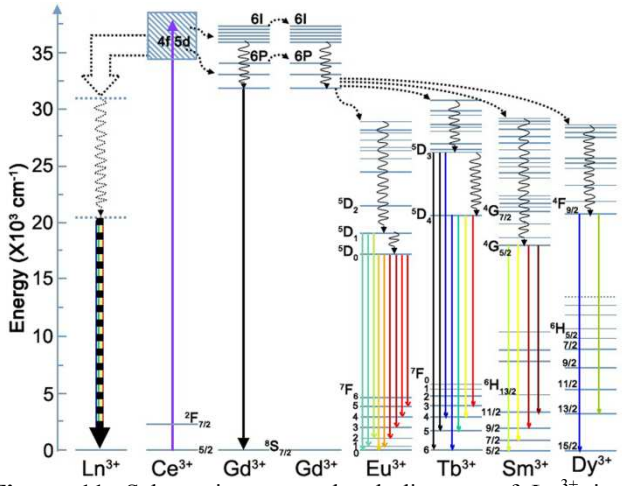

Figure 11. Schematic energy level diagram of Ln^{3+} ions, proposed energy transfer mechanisms. Note that only partial energy levels of Ce^{3+}, Gd^{3+}, and Ln^{3+} (Ln = Eu, Tb, Dy and Sm) are shown for clarity.

4. Conclusions

In conclusion, we have investigated a general hydrothermal in-situ ion-exchange approach for the synthesis of the highly bright and multicolor-emitting $NaGdF_4$ core/shell NCs. The thermodynamic driving force is a key to the formation of $NaGdF_4$. Sensitization of the Eu^{3+}, Tb^{3+}, Dy^{3+} and Sm^{3+} luminescence in the core by Ce^{3+} encapsulated in the shell (via Gd^{3+} sublattice) was realized in the NCs. The dominant effect of $NaGdF_4$ host and the role of sensitizer (Ce^{3+}) were systematic investigated. Ce^{3+} was doped into the crystals as the sensitizer, and with the $NaGdF_4$:5% Ce^{3+} shell coating significant emission enhancement was observed for Gd-based NCs doped of Ln^{3+}. Within $NaGdF_4$:5% Eu^{3+}@$NaGdF_4$@$NaGdF_4$:5% Ce^{3+} nanostructure, PL studies showed that with further increase in the $NaGdF_4$ interlayer thickness, a gradual decrease in emission intensity was observed for the Eu^{3+} ions. The ability to tune PL properties for a rather wide range of activators by using a combination of energy migration and core/shell nanostructural engineering would expand the range of applications for lanthanide-doped NCs. These products with particular characteristics may have the promising potential serving as versatile luminescent phosphors for further application. These studies also pave the way for constructing novel down/upconverison nanomaterials that outperform existing biomarkers for therapeutic and diagnostic imaging applications.

Acknowledgements

This present work was financially supported by the Mineral and Ore Resources Comprehensive Utilization of Advanced Technology Popularization and Practical Research (MORCUATPPR) funded by China Geological Survey (Grant No. 12120113088300); and the Key Technology and

Equipment of Efficient Utilization of Oil Shale Resources, No: OSR-5.

Notes and references

[a] *College of Chemistry, Jilin University, Changchun 130026, P. R. China. *Corresponding author: Shucai Gan; Tel: +86 431 88502259; E-mail address: gansc@jlu.edu.cn (S. Gan).*

*b Teaching Center of Basic Courses, Jilin University, Changchun 130062, PR China. * Corresponding author: E-mail: zoulianchun@126.com*

† Electronic Supplementary Information (ESI) available: XRD patterns of the $NaGdF_4$:5% Ln^{3+} and $Gd(OH)_3$ samples for different reaction time. SEM images of $Gd(OH)_3$ samples for different reaction time. XRD results of the NCs obtained under different ratios of HF/Gd^{3+}. SEM images and XRD of NCs obtained under different ratios of HCl/Gd^{3+} . Dimension parameters of monodispersed $Gd(OH)_3$, $NaGdF_4$, $NaGdF_4$@$NaGdF_4$, $NaGdF_4$@$NaGdF_4$@$NaGdF_4$ nanocrystals. Element maps of $NaGdF_4$@$NaYF_4$:5% Ln^{3+} samples. Emission spectra of the $NaGdF_4$ and $NaGdF_4$@$NaGdF_4$:5 mol% Ce^{3+} and Exitation spectra of the as-prepared $NaGdF_4$:Ln^{3+} .

REFERENCES

1 S. Iijima, *nature*, 1991, **354**, 56.
2 L. Cheng, C. Wang, X. X. Ma, Q. L. Wang, Y. Cheng, H. Wang, Y. G. Li and Z. Liu, *Adv. Funct. Mater.*, 2013, **23**, 272.
3 F. Wang, Y. Zhang, X. P. Fan and M. Q. Wang, *Nanotechnology*, 2006, **17**, 1527.
4 X. H. He and B. Yan, *J. Mater. Chem. C*, 2014, **2**, 2368.
5 F. He, P. P. Yang, D. Wang, N. Niu, S. L. Gai and X. B. Li, *Inorg. Chem.*, 2011, **50**, 4116.
6 Q. Ju, D. T. Tu, Y. S. Liu, R. F. Li, H. M. Zhu, J. C. Chen, Z. Chen, M. D. Huang and X. Y. Chen, *J. Am. Chem. Soc.*, 2012, **134**, 1323.
7 X. Qu, L. Omar, T. B. Le, L. Tetley, K. Bolton, K. W. Cjooi, W. Wang and I. F. Uchegbu, *Langmuir*, 2008, **24**, 9997.
8 Z. Liu, D. Elbert, C. L. Chien, and P. C. Searson, *Nano Lett.*, 2008, **8**, 2166.
9 S. Wang, S. Q. Su, S. Y. Song, R. P. Deng and H. J. Zhang, *CrystEngComm*, 2012, **14**, 4266.
10 J. Ahmed, S. Sharma, K. V. Ramanujachary, S. E. Lofland and A. K. Ganguli, *J. Colloid Interface Sci.*, 2009, **336**, 814.
11 E. Schmidt, A. Vargas, T. Mallat and A. Baiker, *J. Am. Chem. Soc.*, 2009, **131**, 12358.
12 S. H. Yoo and S. Park, *Adv. Mater.*, 2007, **19**, 1612.
13 G. F. Wang, Y. Li, B. J. Jiang, K. Pan, N. Y. Fan, Q. M. Feng, Y. J. Chen and C. G. Tian, *Chem. Commun.*, 2011, **47**, 8019.
14 J. Yu, X. J. Diao, X. J. Zhang, X. F. Chen, X. J. Hao, W. Li, X. H. Zhang and C. S. Lee, *Small*, 2014, **10**, 1125.
15 F. Aldeek, L. Balan, G. Medjahdi, T. Roques-Carmes, J. Malval, C. Mustin, J. Ghanbaja and R. Schneider, *J. Phys. Chem. C*, 2009, **113**, 19458.
16 A. Yahia-Ammar, A. M. Nonat, A. Boos, J. Rehspringer, Z. Asfaria and L. J. Charbonnière, *Dalton Trans.*, 2014, **43**, 15583.
17 A. Aboulaich, M. Geszke, L. Balan, J. Ghanbaja, G. Medjahdi and R. Schneider, *Inorg. Chem.*, 2010, 49, 10940.
18 L. Bonacina, *Pharmaceutics*, 2013, **10**, 783.
19 H. R. Thomas, C. Vall´es, R. J. Young, I. A. Kinloch, N. R. Wilson and J. P. Rourke, *J. Mater. Chem. C*, 2013, **1**, 338.
20 G. Jia, K. Liu, Y. H. Zheng, Y. H. Song, M. Yang and H. P. You, *J. Phys. Chem. C*, 2009, **113**, 6050.
21 H. X Guan, G. X. Liu, J. X. Wang, X. T. Dong, W. S. Yu, *Dalton Trans.*, 2014, **43**,10801.
22 M. Banski, A. Podhorodecki, J. Misiewicz, M. Afzaal, A. L. Abdelhadyc and P. O'Brien, *J. Mater. Chem. C*, 2013, **1**, 801.
23 J. Huan, L. F. Hu and X. S. Fang, *ACS Appl. Mater. Interfaces*, 2014, **6**, 1462.
24 C. F. Hoener, K. A. Allan, A. J. Bard, A. Campion, M. A. Fox, T. E. Malluok, S. E. Webber and J. M. White, *J. Phys. Chem.*, 1992, **96**, 3812.
25 S. Wang, J. Feng, S. Y. Song and H. J. Zhang, *CrystEngComm*, 2013, **15**, 7142.
26 C. W. Lai, Y. H. Wang, C. H. Lai, M. J. Yang, C. Y. Chen, P. T. Chou, C. S. Chan, Y. Chi, Y. C. Chen and J. K. Hsiao, *Small*, 2008, **4**, 218.
27 G. Y. Chen, T. Y. Ohulchanskyy, S. Liu, W. C. Law, F. Wu, M. T. Swihart, H. Ågren and P. N. Prasad, *ACS Nano*, 2012, **6**, 2969.
28 S. H. Tang, J. N, Wang, C. X. Yang, L. X. Dong, D. L. Kong and X. P. Yan, *Nanoscale*, 2014, **6**, 8037.
29 T. Aubert, S. J. Soenen, D. Wassmuth, M. Cirillo, R. V. Deun, K. Braeckmans and Z. Hens, *ACS Appl. Mater. Interfaces*, 2014, **6**, 11714.
30 H. L. Wen, H. Zhu, X. Chen, T. F. Hung, B. L. Wang, G. Y. Zhu, S. F. Yu and F. Wang, *Angew. Chem. Int. Ed.*, 2013, **52**, 1.
31 X. Y. Kuang, H. Liu, W. Y. Hua and Y. Z. Shao, *Dalton Trans.*, 2014, **43**, 12321.
32 D. M. Yang, X. J. Kang, M. M. Shang, G. G. Li, P. Chong, C. X. Li and J. Lin, *Nanoscale*, 2011, **3**, 2589.
33 G. T. Xiang, J. H. Zhang, Z. D. Hao, X. Zhang, Y. S. Luo, S. Z. Lü and H. F. Zhao, *CrystEngComm*, 2014, **16**, 2499.
34 S. Y. Kim, K. Woo, K. Lim, K. Lee and H, S. Jang, *Nanoscale*, 2013, **5**, 9255.
35 F. Wang, X. P. Fan, M. Q. Wang and Y. Zhang, *Nanotechnology*, 2007, **18**, 025701.
36 S. Rodriguez-Liviano, A. I. Becerro, D. Alcántara, V. Grazú, J. M. Fuente and M. Ocaña, *Inorg. Chem.*, 2013, **52**, 647.
37 R. D. Shannon, *Acta. cryst.*, 1976, **A32**, 751.
38 F. Zhang and Zhao, D. Y., *ACS Nano*, 2009, **3**, 159-164.
39 E. M. Goldys, D. T. Krystyna, J. J. Sun, D. Dosev, I. M. Kennedy, S. Yatsunenko and M. Godlewski, *J. Am. Chem. Soc.*, 2006, **128**, 14498.

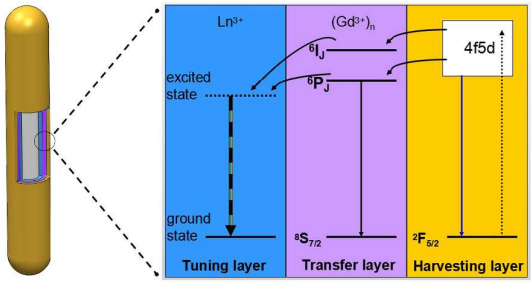

Multicolour photoluminescence were achieved in gadolinium-based core/shell nanotube structure via energy migration of $Ce^{3+}\rightarrow Gd^{3+}\rightarrow Ln^{3+}$ and $Ce^{3+}\rightarrow Ln^{3+}$ (Ln = Eu, Tb, Dy and Sm) in separated layers.